Science of the Total Environment 911 (2024) 168494

Contents lists available at ScienceDirect

Science of the Total Environment

journal homepage: www.elsevier.com/locate/scitotenv

Greater local cooling effects of trees across globally distributed urban green spaces

Jiyoung Kim *, Abdou Khouakhi, Ronald Corstanje, Alice S.A. Johnston

Cranfield Environment Centre, School of Water, Energy and Environment, Cranfield University, Cranfield, Bedfordshire MK43 0AL, UK

HIGHLIGHTS

- We compiled local in-situ air temperatures for global urban green spaces (UGS).
- Temperature differential relationships with climate, plant and urban variables were analysed.
- A robust hierarchical linear-mixed effect model was used for parsimony.
- UGS demonstrated stronger local cooling in milder climates with higher plant growth.
- Trees dominated UGS cooling effects globally, compared to grass and green roofs and walls.

GRAPHICAL ABSTRACT

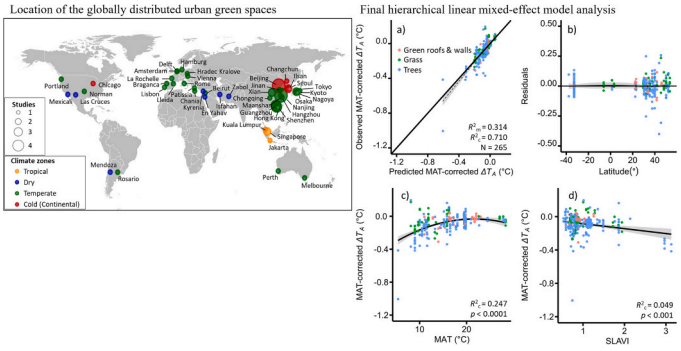

ARTICLE INFO

Editor: Shuqing Zhao

Keywords:
Urban heat
Green infrastructure
Background climate
Heat mitigation
Vegetation index

ABSTRACT

Urban green spaces (UGS) are an effective mitigation strategy for urban heat islands (UHIs) through their evapotranspiration and shading effects. Yet, the extent to which local UGS cooling effects vary across different background climates, plant characteristics and urban settings across global cities is not well understood. This study analysed 265 local air temperature (T_A) measurements from 58 published studies across globally distributed sites to infer the potential influence of background climate, plant and urban variables among different UGS types (trees, grass, green roofs and walls). We show that trees were more effective at reducing local T_A, with reductions 2–3 times greater than grass and green roofs and walls. We use a hierarchical linear mixed effects model to reveal that background climate (mean annual temperature) and plant characteristics (specific leaf area vegetation index) had the greatest influence on cooling effects across UGS types, while urban characteristics did not significantly influence the cooling effects of UGS. Notably, trees dominated the overall local cooling effects across global cities, indicating that greater tree growth in mild climates with lower mean annual temperatures has the greatest mitigation potential against UHIs. Our findings provide insights for urban heat mitigation using UGS interventions, particularly trees across cities worldwide with diverse climatic and environmental conditions and highlight the essential role of trees in creating healthy urban living environments for citizens under extreme weather conditions.

* Corresponding author at: Bullock Building, Cranfield University, Cranfield, Bedfordshire MK43 0AL, UK.
E-mail address: jiyoung.kim@cranfield.ac.uk (J. Kim).

https://doi.org/10.1016/j.scitotenv.2023.168494
Received 19 August 2023; Received in revised form 18 October 2023; Accepted 9 November 2023
Available online 18 November 2023

1. Introduction

Today, over half of the global population lives in cities, and this trend is expected to rise to 70 % by 2050 (United Nations. Department of Economic and Social Affairs, Population Division, 2019). Urban populations face increasing pressure from extreme heat, as rapid development and global climate change intensify urban heat islands (UHIs) (Krayenhoff et al., 2018; Mora et al., 2017; Zhao et al., 2018). Developing UHI mitigation strategies is thus crucial for healthy and resilient urban systems in the future. Most UHI studies measure differences in land surface temperature (LST) between urban and surrounding suburban or rural areas using remote sensing data (Estoque et al., 2017; Imhoff et al., 2010; Manoli et al., 2019). These studies have revealed that UHIs vary in magnitude from 0.8 to 8.0 °C (Imhoff et al., 2010; Manoli et al., 2019), are stronger in summer and during night-time (Gartland, 2008), and are strongly influenced by urban size, local climate, urbanisation gradients and impervious surface area (Estoque et al., 2017; Li et al., 2019; Manoli et al., 2019; Shi et al., 2023; Varquez and Kanda, 2018; Zhao et al., 2014). However, we currently lack an understanding of how these disparate UHI findings can be applied to urban interventions (e.g., green infrastructure) that aim to reduce urban heat at local scales across global cities.

Urban green spaces (UGS) have the potential to reduce the temperature of surrounding areas through evapotranspiration, the provision of shade, and increased albedo (Bowler et al., 2010). UGS has thus been extensively studied as a UHI mitigation strategy for diverse UGS types (e.g., parks, grass, green roofs and walls) according to various methods (e.g., field measurements, remote sensing and model simulations) (Balany et al., 2020; Bartesaghi Koc et al., 2018; Saaroni et al., 2018). However, the magnitude of UGS cooling effects varies substantially with the UGS type, urban and climate context (Manoli et al., 2019; Shi et al., 2023; Su et al., 2022). For instance, greater cooling effects have been identified for urban trees compared to grasslands (Bartesaghi-Koc et al., 2020), at higher background temperatures (Su et al., 2020), and for drier intra-climate regions (Manoli et al., 2019). Most studies of local UGS cooling effects have also focused on a limited scope of locations, particular UGS types and/or a range of methods that are not directly comparable (Bartesaghi Koc et al., 2018; Su et al., 2020), restricting the identification of UGS cooling effects that are applicable across globally diverse urban areas.

Quantifying the local cooling effects of UGS across diverse urban and climatic contexts on a global scale would guide a better understanding of the role of UGS in UHI mitigation. The application of the remote sensing approaches used to study landscape-scale UHIs, however, is often restricted by the micro-scale implementation of UGS in real urban areas. Field measurements, empirical observations of air temperature (T_A) using sensors, weather stations and thermistors, provide a more direct measure of UGS's instantaneous and real-world effects on temperature (Bowler et al., 2010). A recent synthesis of observational field data on a global scale demonstrated vegetation growth, seasonality and latitude as the key driving factors of UGS cooling effects (Su et al., 2020). Subsequent statistical analysis of these observations partially explained the influence of key interacting factors (evapotranspiration and leaf area index) on point T_A measurements across globally distributed sites and UGS types according to polynomial and additive regression models (Su et al., 2022). A unified understanding of the global cooling potential of UGS, however, will depend on more parsimonious approaches to disentangling these complex non-linear patterns in T_A.

In this study, we compiled a global dataset of locally measured T_A differentials (ΔT_A) between various UGS types (trees, grass and green roofs and walls) and neighbouring urban spaces (impervious surfaces). ΔT_A measurements were then supplemented with climatic, plant and urban metrics to reveal whether the effects of UGS on local T_A follow similar trends to those identified for UHIs on a global scale. Taking the observations from local to global urban heat studies outlined above, we hypothesised that background climate influences the magnitude of ΔT_A through large-scale controls on vegetation physiology, while plant and urban characteristics influence the direction (positive or negative) of ΔT_A across globally distributed sites. That is, we expect greater plant productivity in temperate and wet climates to promote local UGS cooling effects, while urban areas with greater impervious surfaces outweigh the cooling benefits of UGS due to greater heat absorption.

2. Methods

2.1. Data collection

We collected T_A measurements for green and urban spaces across globally distributed sites using PRISMA systematic literature review guidance (Page et al., 2021). The systematic literature review was conducted using Web of Science for all peer-reviewed journal articles available until April 2023 with no restrictions on start date or location. The following search terms were used to include all studies reporting UGS types and a measure of urban heat and/or cooling: (green infrastructure OR green space* OR sustainable drainage system* OR water sensitive urban design OR green*roof OR living roof* OR green*wall OR vertical green* OR urban garden OR urban*farm OR urban forest) AND (urban heat island OR urban*cooling OR climate*mediation OR climate*regulation) AND (air temperature* OR heat intensity*). The following criteria to screen and select appropriate studies were used: (1) only field measurements were selected, and laboratory incubation studies or computer model outputs were not included; (2) only T_A effects were considered for consistency between studies; (3) at least one T_A dataset for both green and urban spaces that can calculate ΔT_A between green and urban spaces is reported; and (4) studies only written in English are considered. Based on the result of PRISMA, a total of 58 peer-reviewed articles with 277 measurements were included that quantified the effect of UGS on T_A (Fig. 1). Additionally, we removed (i) the temperature data collected from water sources due to few data points (n = 4) and (ii) outliers that were identified from the trends of collected ΔT_A, excluding the range of <-5.5 to >3 °C (n = 8). Finally, a total of 265 observed temperature measurements from 58 published studies (Table S1) were used for the data analysis outlined in the following sections.

2.1.1. Site-specific field measurements

T_A observations for green and urban spaces were retrieved directly from tables and text within each paper, or from plots using WebPlotDigitizer software (version 4.6) (Rohatgi, 2022). We included T_A observations exclusively from sunny days and excluded data from cloudy and rainy days to ensure the quality of remote sensing data for assessing plant characteristics at the measurement sites. As measurement heights of T_A vary across the published papers, the effect of measurement heights on ΔT_A was tested using one-way ANOVAs. The result showed no significant interaction between ΔT_A and measurement heights (Fig. S1). In addition, 25 ΔT_A observations (9.4 % of 265 total ΔT_A observations) were measured in shaded conditions, ranging from -4.32 to -0.03 °C, which fell within the range of ΔT_A observations after removing outliers. Alongside T_A, the dataset also included basic site information such as city, country, latitude, longitude, measurement time/periods, experimental method, climate classification based on Köppen–Geiger climate classification system (tropical, dry, temperate and cold (continental)) (Beck et al., 2018). UGS were classified into three common types: trees, grass and green roofs and walls (Bartesaghi Koc et al., 2018). Here, grass included low UGS types such as grass, shrubs and forbs, and trees encompassed urban forests, parks, street trees and trees mixed with low UGS. Measurement times for day and night in each city were determined by sunrise and sunset times (https://www.sunrise-and-sunset.com/en/sun), which were selected based on the starting date of the T_A measurements.

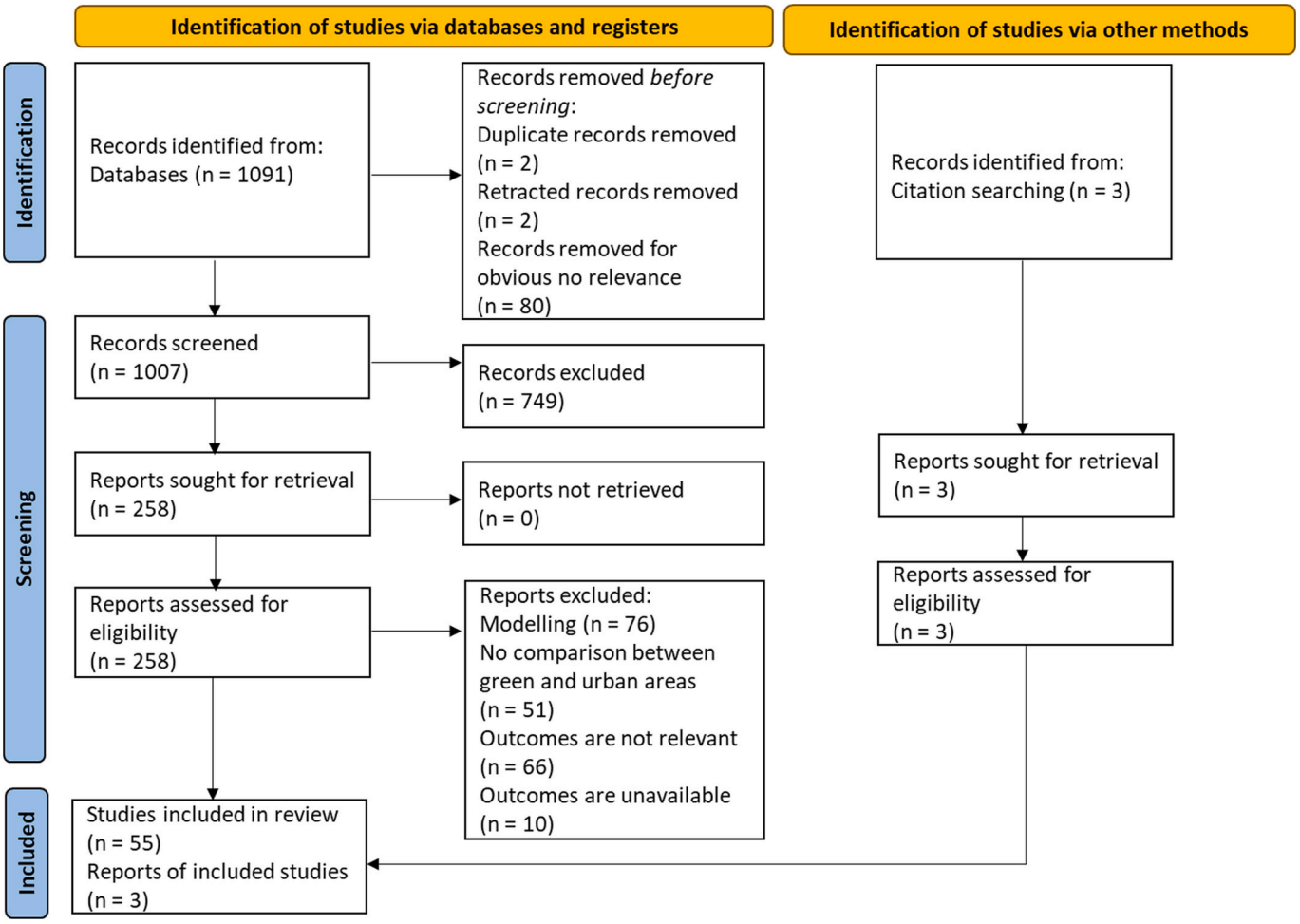

Fig. 1. PRISMA flow diagram of the systematic literature review process for identification, screening and inclusion of studies on in-situ temperature measurements on urban green space areas across global cities.

2.1.2. Background climate data

Background climate was characterised according to variations in annual and monthly temperature and precipitation measurements. If mean annual temperature (MAT, °C), minimum/maximum annual temperature (MinAT/MaxAT, °C), and mean annual precipitation (MAP, mm) measurements were missing from the corresponding paper they were extracted for the study site/s (at the city level) and year from the World Bank Group (https://climateknowledgeportal.worldbank.org/). Temperature variation (MATv, °C) was calculated using MinAT and MaxAT (MATv = MaxAT − MinAT). Additionally, monthly temperature data were included to consider monthly temperature variation for background climate. Mean, minimum and maximum temperature by month (MTM/MinTM/MaxTM, °C) and mean precipitation by month (MPM, mm) across the study sites were collected via the Climate Data (https://en.climate-data.org/). The months for MTM, MinTM, MaxTM and MPM were based on T_A measurement period from each study to ensure consistency of observed T_A and meteorological conditions during the T_A observation periods. If T_A was observed for more than two months, MTM, MinTM and MaxTM were averaged and MPM was accumulated for the entire observation period.

2.1.3. Plant and urban characteristics data

Plant and urban characteristics data were collected using open-access remote sensing data. Landsat satellite imagery was used as it covers the broader data period from 1972 to the present compared to other sources such as MODIS and Sentinel (Adab et al., 2016; Zhou et al., 2019). Owing to the data availability of Landsat, two Landsat imagery collections were used: Landsat 8 data collection for T_A measurements taken on or after April 11, 2013, and Landsat 7 data collection for T_A measurements preceding that date. Both image collections are atmospherically corrected and meet geometric and radiometric quality requirements with 30 m spatial resolution. Average values for each vegetation index were computed in Google Earth Engine using the Python *eemont* package (Montero, 2021). As a proxy of plant characteristics vegetation indices were used including the Normalized Difference Vegetation Index (NDVI), Enhanced Vegetation Index (EVI), Normalized Difference Moisture Index (NDMI), Leaf Area Index (LAI) and Specific Leaf Area Vegetation Index (SLAVI). Normalized Difference Built-up Index (NDBI) was further used as an urban characteristic proxy for each site. These indices were selected in relation to the function of evapotranspiration and the shading benefits of UGS (Table 1). Robust vegetation (NDVI, EVI and SLAVI) and plant water content (NDMI) were determined based on evapotranspiration, which is indicative of active transpiration. Leaf density (LAI) and greenness (NDVI and EVI) were chosen for shading benefits, which contribute to effective shading by intercepting solar radiation. All indices were captured from the remotely sensed imageries in a buffer of a 500 m radius around the observed site in the city, which was chosen based on the strong relationship between T_A and LST in a wider environment (Unger et al., 2009). A cloud and cloud shadow masking based on the quality assessment band included in Landsat surface reflectance (SR) products was applied using *eemont* to ensure that the imagery used for index calculation is not affected by cloud cover (Montero, 2021). During the T_A observation periods, the likelihood of coming across Landsat images at specific sites varied due to

Table 1
Selected vegetation and urban indices as proxies of plant and urban characteristics used in the study, indicating index abbreviation, index name, plant characteristic, formula and reference.

Index abbreviation	Index name	Plant characteristic	Formula	Reference
NDVI	Normalized Difference Vegetation Index	Plant greenness	(NIR − R)/(NIR + R)	(Wilson and Sader, 2002)
NDMI	Normalized Difference Moisture Index	Plant water content	(NIR − SWIR1)/(NIR + SWIR1)	
EVI	Enhanced Vegetation Index	Plant Greenness	2.5 × ((NIR − R)/(NIR + 6 × R − 7.5 × B + 1))	(Li et al., 2018)
LAI	Leaf Area Index	Leaf density	−ln[(0.69 − SAVI*) / 0.59] / 0.91	(Biudes et al., 2014)
SLAVI	Specific Leaf Area Vegetation Index	Plant size and growth	NIR / (R + SWIR2)	(Lymburner et al., 2000)
NDBI	Normalized Difference Built-up Index	Urban built-up area	(SWIR − NIR)/(SWIR + NIR)	(Zha et al., 2003)

Abbreviations in the formula: near infrared (NIR), red (R), blue (B), shortwave infrared 1 (SWIR1) and shortwave infrared 2 (SWIR2).
* SAVI (Soil Adjusted Vegetation Index) = ((NIR − R) / (NIR + R + 0.5)) * (1 + 0.5) (Huete, 1988).

factors like the absence of images (given Landsat's 2-week revisit time) or cloud and shadow cover. To address this, we chose to compute average indices over a one-year duration, using exclusively cloud and shadow-free images. Annual vegetation indices smooth out the seasonality effects, making it easier to see the underlying land use/cover patterns for globally distributed sites. Using annual averages provided a robust approach, ensuring data consistency, quality and availability across all sites. This enhanced our ability to highlight vegetation and non-vegetation patterns more effectively throughout the T_A observation period. In addition, data for the human population of the city in the study were collected from the online database https://citypopulation.de/.

2.2. Data summary

A total of 265 ΔT_A measurements between green and urban spaces were used for the data analysis outlined in the following section. These measurements were extracted from 58 studies across 46 cities and 23 countries between 2002 and 2021 (Fig. 2; Fig. S2). Of 46 cities, 31, 7, 5 and 3 cities were located in temperate, dry, cold (continental) and tropical climates, respectively. Broad UGS types were classified into three distinct types: trees (35 studies), grass (17 studies) and green roofs and walls (16 studies). The sampling times for temperature observations were during both the daytime and night-time (29 studies), during the daytime (28 studies) and the night-time (1 study). The measurement methods used for temperature were mainly sensors (36 studies), followed by thermistors (10 studies), weather stations (9 studies) and mobile (3 studies). Here, sensors are devices that measure air temperature using the principles of electrical resistance, while thermistors rely on the temperature-dependent resistance of semiconductor materials. Mobile is classified under sensors, but they utilise sensors to measure air temperature while being mobile (e.g., bicycles, cars, and drones).

2.3. Data analysis

Data analysis was performed in the R software environment (R Core Team, 2022) and focused on explaining relationships between local ΔT_A between green and urban spaces. First, a global trend of UGS cooling effects on local ΔT_A was presented across MAT (<10 °C, 10–20 °C,

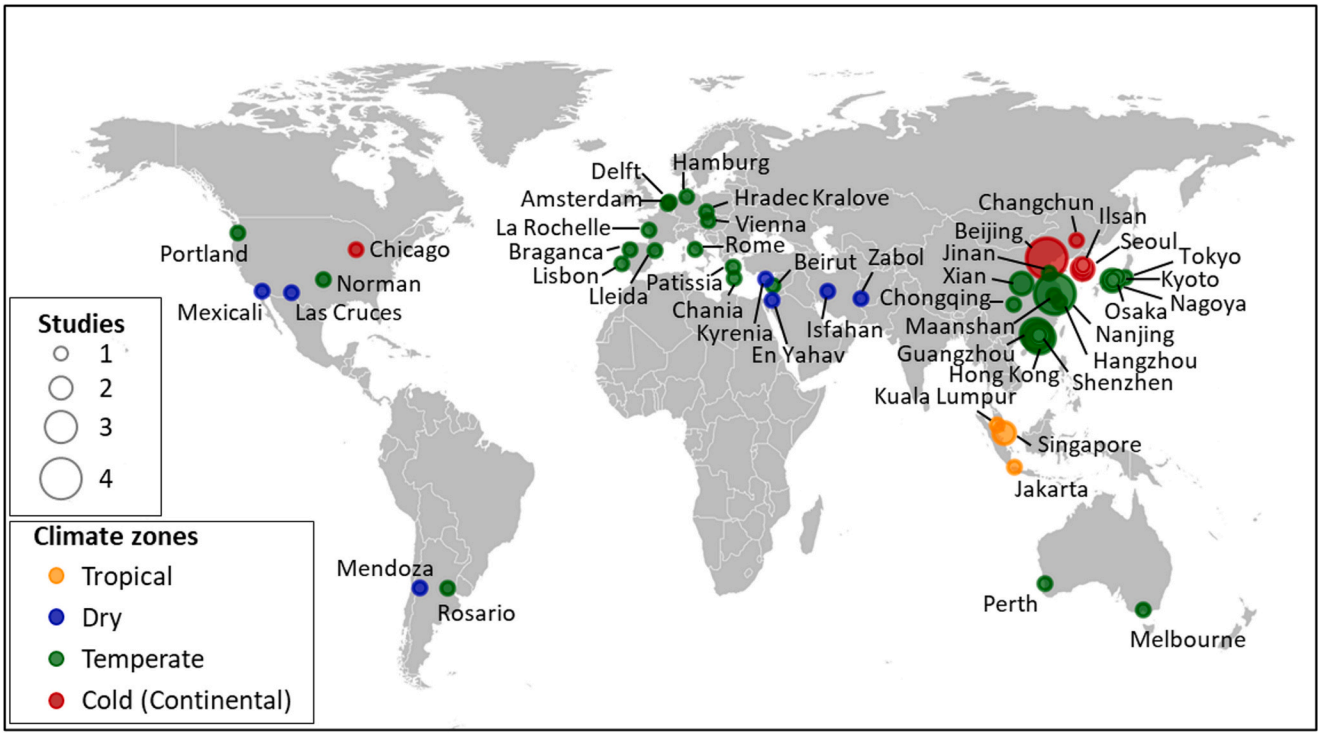

Fig. 2. Location of the globally distributed urban green spaces included in this study, representing 265 local air temperature differentials between green spaces and urban areas (impervious surfaces) from 58 studies across 46 cities (symbol size indicates the number of studies as in the legend). The climate zones were classified into four groups according to the Köppen–Geiger climate classification system (tropical (yellow), dry (blue), temperate (green) and cold (continental) (red)).

20–30 °C), latitude (40–30°S, 30–0°S, 0–30°N, 30–40°N, >40°N), UGS types (trees, grass and green roofs and walls) and climate zones (tropical, dry, temperate and cold (continental)). Following this, ΔT_A was investigated across broad categorical variables (MAT, latitude, UGS types, climate zones, sampling times (day and night) and measurement methods (mobile, sensor, thermistor and weather station)) before a hierarchical model was used to disentangle the importance of various environmental controls on local ΔT_A across globally distributed sites.

2.3.1. Response ratios between local green and urban spaces

Differences in observed T_A between broad groups including MAT, latitude, UGS types, climate zones, sampling times and measurement methods were analysed in the dataset. To compare response ratios among these broad groups, the standardised mean difference of observed T_A between green and urban spaces was calculated (SMD = ln (T_A_green / T_A_urban)) and used as a response variable (Fig. S3a). Effects were tested using one-way ANOVAs and taking $p < 0.05$ to support a significant difference between groups.

2.3.2. Hierarchical model of UGS controls on ΔT_A

A hierarchical linear mixed-effects model was used to test the influence of environmental and urban characteristics on ΔT_A measurements. Here, in regions with higher background temperatures, larger temperature differences are observed, while in regions with lower background temperatures, smaller differences are observed. To facilitate the comparison of temperature data across various global locations, it is important to normalise observed T_A by correcting ΔT_A by MAT according to: MAT-corrected ΔT_A = (T_A_green / MAT) − (T_A_urban / MAT) (Fig. S3b) (Parishwad et al., 1998).

We use a hierarchical modelling approach to test the importance of background climate, plant and urban characteristics on MAT-corrected ΔT_A across globally distributed sites. To evaluate the effect of using MAT-corrected ΔT_A as a response variable, we also run the hierarchical model for the SMD between T_A measurements in local green and urban spaces. The hierarchy of terms tested explains the effects of 'controls' before 'function'. That is, variables that cause variations in multiple UGS and urban properties (e.g., background climate) are added first, so that if 'controls' explain the variation in 'functions' (e.g., plant characteristics) then the addition of these variables does not improve the model likelihood. All models were linear mixed-effects models, with latitude (N = 46) considered as a random effect across 265 observations, using the *lme4* package (Bates et al., 2015). The random effects in the hierarchical mixed effects model account for spatial autocorrelation, which reflects the proximity of latitude values to one another (e.g., north vs south), rather than indicating positive and negative values for the north and south hemispheres.

Hierarchical terms, which include groups of variables associated with the overall term, were added in the following order: background climates (MAT, MAP, MTM, MinTM, MaxTM, MATv and MPM), plant characteristics (NDVI, EVI, NDMI, LAI and SLAVI) and urban characteristics (human population and NDBI). Each variable was added as a linear or quadratic (non-linear) term, with and without interactions between variables. For a list of variable combinations and procedures tested by the model see Table S2. Models were then compared by testing their influence on the goodness of fit (Akaike's Information Criterion, AIC), model likelihood (Chi-square $p < 0.05$) and parsimony (ΔAIC > 5 for additional degrees of freedom). Models that met these criteria were tested with the subsequent hierarchical terms and groups of variables. Pseudo-marginal (fixed effect) and conditional (fixed and random effect) R^2 values for the hierarchical models were calculated using the MuMIn package in R (Bartoń, 2023). In addition, isolated fixed effects of the final hierarchical linear mixed-effects model were tested using *lm* function which is the base R package for general linear models.

3. Results

3.1. Cooling effects of UGS on local T_A

Across globally distributed sites ΔT_A varied from −5.4 to 2.6 °C with a median of −1.2 °C, where negative values indicate a cooling effect (Fig. S3c). 85 % of all observed ΔT_A measurements present a cooling effect of UGS (i.e., $\Delta T_A < 0$). ΔT_A showed distinctions across different MAT, latitude, UGS type and climate zone groups during the daytime and night-time (Fig. 3). ΔT_A in each group tends to exhibit greater cooling effects during the daytime than at night-time. Specifically, UGS had a greater cooling effect during both daytime and night-time at lower MATs (<10 °C), with ΔT_A of −1.9 ± 0.30 °C in the day and −1.5 ± 0.44 °C at night. ΔT_A was reduced at higher MATs (20–30 °C, daytime: −0.7 ± 0.16 °C; night-time: ΔT_A = −0.6 ± 0.26 °C) (Fig. 3a). The most substantial cooling effects were observed during the daytime at the lower southern latitude of 30–0°S (ΔT_A = −2.0 ± 0.33 °C), followed by the higher northern latitude of 30–40°N (ΔT_A = −1.7 ± 0.13 °C) and >40°N (ΔT_A = −1.4 ± 0.25 °C). During night-time, the greatest cooling effects occurred at the higher southern latitude (40–30°S: ΔT_A = −1.9 ± 0.24 °C), which stands out from the overall trend of greater cooling effects in the day (Fig. 3b). This exceptional night-time cooling was determined by a specific study attributed to increased transpiration from street trees, countering the absorbed heat released by buildings (Coronel et al., 2015). From the broad UGS types, trees had a greater cooling effect (daytime: ΔT_A = −1.5 ± 0.10 °C; night-time: ΔT_A = −1.5 ± 0.18 °C) followed by grass (daytime: ΔT_A = −0.8 ± 0.21 °C; night-time: ΔT_A = −0.6 ± 0.25 °C) and green roofs and walls (daytime: ΔT_A = −0.6 ± 0.23 °C; night-time: ΔT_A = −0.4 ± 0.13 °C) (Fig. 3c). Cold (continental) climate regions during both daytime and night-time exhibited pronounced cooling effects (daytime: ΔT_A = −1.9 ± 0.22 °C; night-time: ΔT_A = −1.1 ± 0.41 °C). Greater differences between daytime and night-time in dry climate regions (daytime: ΔT_A = −1.4 ± 0.34 °C; night-time: ΔT_A = 0.5 ± 0.31 °C) were observed, whereas smaller differences were observed in temperate climate regions (daytime: ΔT_A = −1.2 ± 0.10 °C;

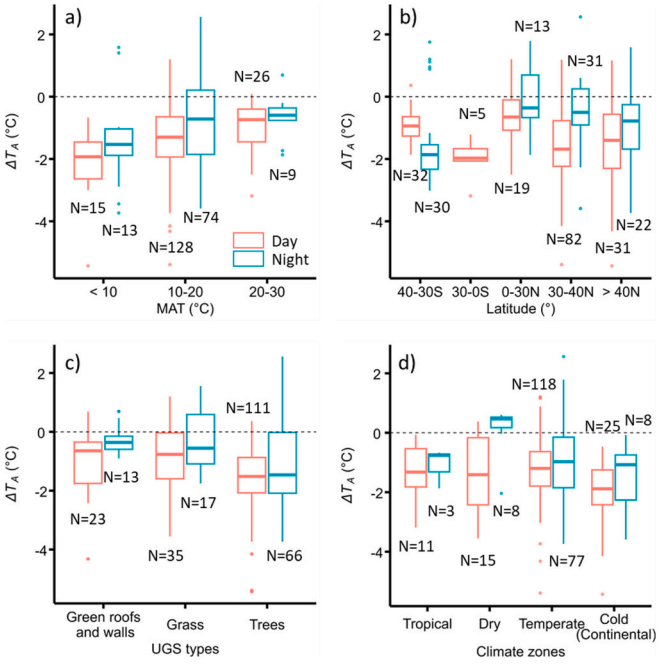

Fig. 3. The local air temperature differential (ΔT_A) variability by sampling times: day (light red boxes) and night (light blue boxes) across globally distributed sites for different a) mean annual temperature (MAT), b) latitude, c) urban green space (UGS) types, and d) climate zones. The number of ΔT_A is indicated for each bar (total N = 265).

night-time: $\Delta T_A = -1.0 \pm 0.16$ °C) (Fig. 3d).

3.2. T_A response ratios

SMD between T_A measurements in local green and urban spaces differed significantly with MAT (Fig. 4a; ANOVA: $F = 8.849, p < 0.001$), latitude (Fig. 4b; ANOVA: $F = 3.626$, $p < 0.01$) and UGS types (Fig. 4c; ANOVA: $F = 4.176$, $p < 0.05$), but did not differ significantly across other groups including sampling times, climate zones or measurement methods (Fig. 4d, e & f; Table S3).

3.3. Hierarchical model of UGS effects on local T_A

A hierarchical model was used to test the importance of various environmental and urban controls on global relationships between MAT-corrected ΔT_A and background climate, plant and urban characteristics. Addition of two terms (MAT and SLAVI) improved the hierarchical model goodness of fit and likelihood in comparison to the null model, with the condition that adding an additional term must be met with a goodness of fit of ΔAIC > 5 and Pr(>Chisq) < 0.05 (Table 2; Table S4). No urban characteristics met the model selection criteria. We also tested the hierarchical model using SMD as the response variable and found the influence of climate to be masked, with selected hierarchical terms restricted to plant characteristics (Table S5).

The final hierarchical model included quadratic MAT and SLAVI terms, with these fixed effects explaining ~31 % of the variation in MAT-corrected ΔT_A across globally distributed sites (Fig. 5). Alongside the fixed effect terms, addition of latitude as a random effect to account for spatial autocorrelation between measurements explains an overall ~71 % of variation in MAT-corrected ΔT_A observations (Fig. 5a & b). Thus, while MAT and SLAVI capture general trends in the direction and magnitude of background climate and plant characteristics on MAT-corrected ΔT_A, site-specific conditions (e.g., different UGS sizes, built-up areas and building heights) leading to high variation in measurements at single sites were not captured in the hierarchical model (Fig. 5b). Representation of the isolated fixed effects in Fig. 5c & d indicates that, in general, the cooling benefits of UGS were greater at lower MATs and at higher SLAVI values (Table S6).

3.4. Cooling effects of different UGS types

The hierarchical model aimed to explain variations in the cooling benefits of UGS according to general background climate, plant and urban characteristics. Here, we investigate whether the fixed effects of MAT and SLAVI varied significantly between UGS types (Fig. 6; Table S7). Relationships between MAT-corrected ΔT_A with MAT and SLAVI were only significant for trees (Fig. 6a & d), whereas no clear relationship existed for grass (Fig. 6b & e) and green roofs and walls (Fig. 6c & f). Fixed effect relationships with MAT-corrected ΔT_A identified by the hierarchical model in Table 2 and Fig. 5 above were, thus, dominated by the response of trees including urban forests, parks, street trees and trees mixed with low UGS to both background climate and plant characteristics (Table S8).

4. Discussion

Our synthesis of ΔT_A between UGS and urban spaces across globally distributed sites (Fig. 2) identified a median cooling effect of −1.2 °C, which was much higher for urban trees (−1.5 °C) than grass (−0.7 °C) or green walls and roofs (−0.6 °C) during the daytime (Figs. 3 & 4; Fig. S3). We used the global dataset of local ΔT_A measurements compiled from urban heat studies to test the influence of background climate, plant and urban characteristics on UGS cooling effects. Using a robust hierarchical model that favours parsimony we found climate and plant characteristics had a strong influence on ΔT_A, with the cooling effects of UGS increasing at lower MATs and higher SLAVIs (Fig. 5 & Table 2). Trees dominated these global relationships between ΔT_A and MAT and SLAVI, whereas no clear relationships existed for the cooling effects of grass and green roofs and walls (Fig. 6).

4.1. Local ΔT_A across globally distributed cities

In our analysis, the local ΔT_A ranged from −5.4 to 2.6 °C across all sites. These findings align with similar global studies by Su et al. (2020), which reported local ΔT_A ranging from −9.7 to 5.2 °C worldwide, as well as by Marando et al. (2022), which reported a range of −3.3 to 5.2 °C across Europe. In general, UGS cooling effects were greater during the daytime compared to night-time due to active plant evapotranspiration and shading intervention during the day. However, an exceptional night-time trend was observed in our study at higher southern latitudes (40–30°S: $\Delta T_A = -1.9 \pm 0.24$ °C), influenced by exceptional raw data from a specific study due to increased transpiration from street trees, countering the absorbed heat released by buildings (Coronel et al., 2015). In addition, there is no data at night-time observed at southern latitudes between 30 and 0°S. To ensure a fair comparison between latitude groups, more representative studies should be conducted in the southern latitude regions. The local ΔT_A for urban trees in our study (−1.5 °C) was slightly lower than previous findings for trees in general (urban parks: −1.7 °C; street trees: −1.3 °C), but grass (−0.7 °C) showed slightly higher cooling effects than previous findings for grass (−0.6 °C) (Su et al., 2020). These differences can be attributed to the broader categories of trees applied in our analysis, such as forests, trees mixed with low plants and street trees, while grass-type included broader low plants such as shrubs and forbs.

4.2. Effects of background climate on UGS cooling

Background temperature had the largest influence on UGS cooling effects globally, particularly in milder climates with MAT < 10 °C (Figs. 3, 4 & 5). Several larger-scale climate effects on vegetation growth and ecophysiological processes could underpin this relationship. Longer growing seasons, greater water availability and the absence of severe temperature extremes, for instance, support wider spread and abundant vegetation growth in milder climates by providing optimal conditions for plant development (Winbourne et al., 2020). Greater plant richness in milder climates can also support more resilient GS, in response to extremes such as droughts and floods (Iio et al., 2014). However, the applicability of this relationship may vary in managed urban environments, such as selecting plant species and providing irrigation. We also found the cooling benefits of UGS to be more pronounced at MAT's below 20 °C. Previous research in the continental USA by Wang et al. (2020) showed that regions with MAT ranging from 8.0 to 16.6 °C exhibited greater UGS cooling effects due to stronger ecophysiological mechanisms, such as evapotranspiration, shading, reflection and radiative absorption. However, there is a wide variation reported from other similar studies, suggesting that UGS have greater cooling effects in regions with higher MAT and during heat waves due to the increased sensitivity of UGS cooling capacity to temperature changes (Su et al., 2020; Wang et al., 2019). In our analysis, seasonal temperatures (MTM, MinTM and MaxTM) did not show a significant relationship with observed T_A measurements in the climatic hierarchical term. This finding suggests that annual climate variables and vegetation indices better reflect variations in temperature and plant constraints on UGS cooling effects across globally distributed sites. The annual vegetation data effectively smooth out seasonal variations, which can vary significantly based on the specific geographical location of the site. Although our analysis highlights the significant influence of background temperature, particularly in regions with milder temperatures in regulating the magnitude of local T_A, considering other environmental factors, such as water availability, albedo, and plant species and seasonality is necessary for gaining a comprehensive understanding of the UGS cooling effects on a global scale.

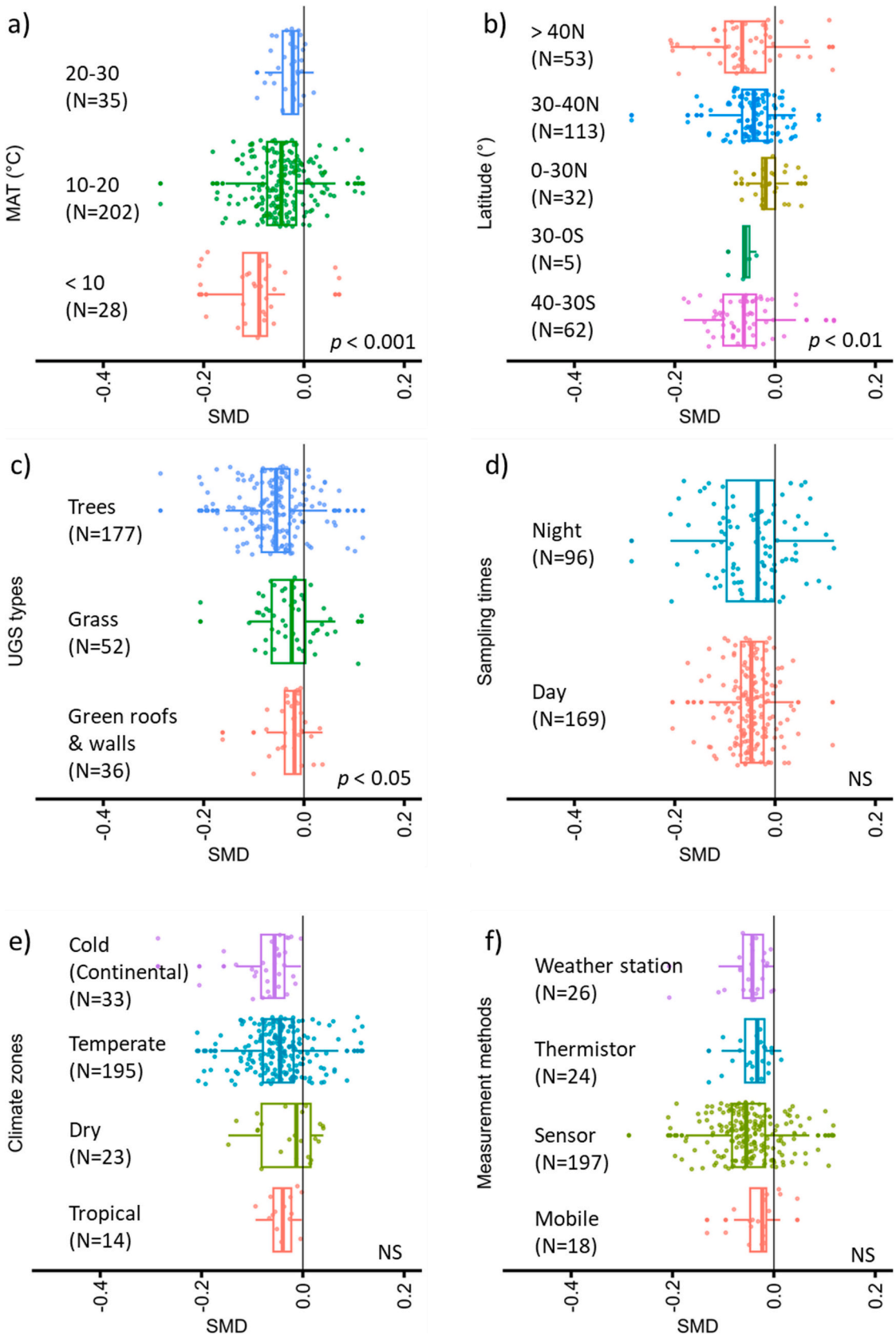

Fig. 4. The relationships between the standardised mean difference (SMD) of observed local air temperatures in green and urban spaces across globally distributed sites (total N = 265) and different a) mean annual temperature (MAT), b) latitude, c) urban green space (UGS) types, d) sampling times, e) climate zones, and f) measurement methods. NS indicates non-significant interactions between SMD and each group.

Table 2
Comparison of models used to explain global patterns in MAT-corrected ΔT_A between green and urban spaces, indicating the hierarchical term, model (if selected) and measures of model goodness of fit and likelihood (total $N = 265$). NA indicates that addition of the hierarchical term did not improve the model fit to the data. Overall goodness of fit is determined by AIC values, where lower AICs indicate a better fit to the data. ΔAICs present the difference in AIC values between each selected model and the final hierarchical model. R^2m and R^2c indicate pseudo-marginal (fixed effect only) and conditional (fixed and random effect) R^2 values for the hierarchical models, respectively. Q indicates that the term selected was quadratic.

Hierarchical term	Variable	*df*	R^2m	R^2c	Pr(>Chisq)	AIC	ΔAIC
Null		3	0	0.629		−505.29	32.68
Background climate (MAT, MAP, MTM, MinTM, MaxTM, MATv, MPM)	MAT (Q)	5	0.284	0.648	<0.0001	−524.24	13.73
Plant characteristics (NDVI, EVI, NDMI, LAI, SLAVI)	SLAVI	6	0.314	0.710	<0.0001	−537.97	0
Urban characteristics (Population, NDBI)	NA						

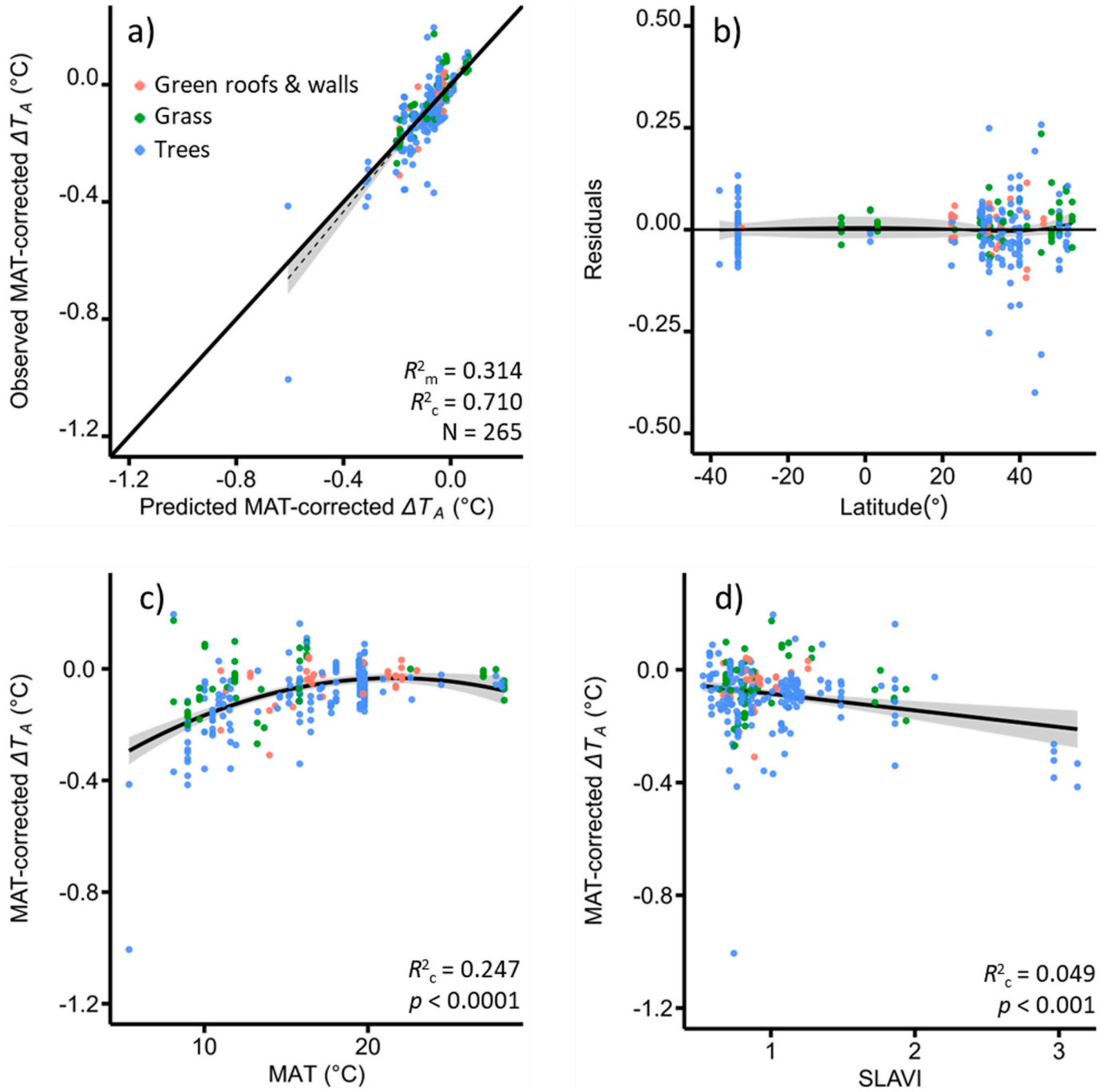

Fig. 5. Final hierarchical linear mixed-effects model (total N = 265) a) predictions compared to observed local air temperatures in green and urban spaces corrected for MAT; b) model residuals against latitude, with the lowess fit (black line with shaded area showing standard error) displaying deviations between model predictions and observed temperature differences; together with the fixed relationships between local air temperature differences and c) MAT and d) SLAVI.

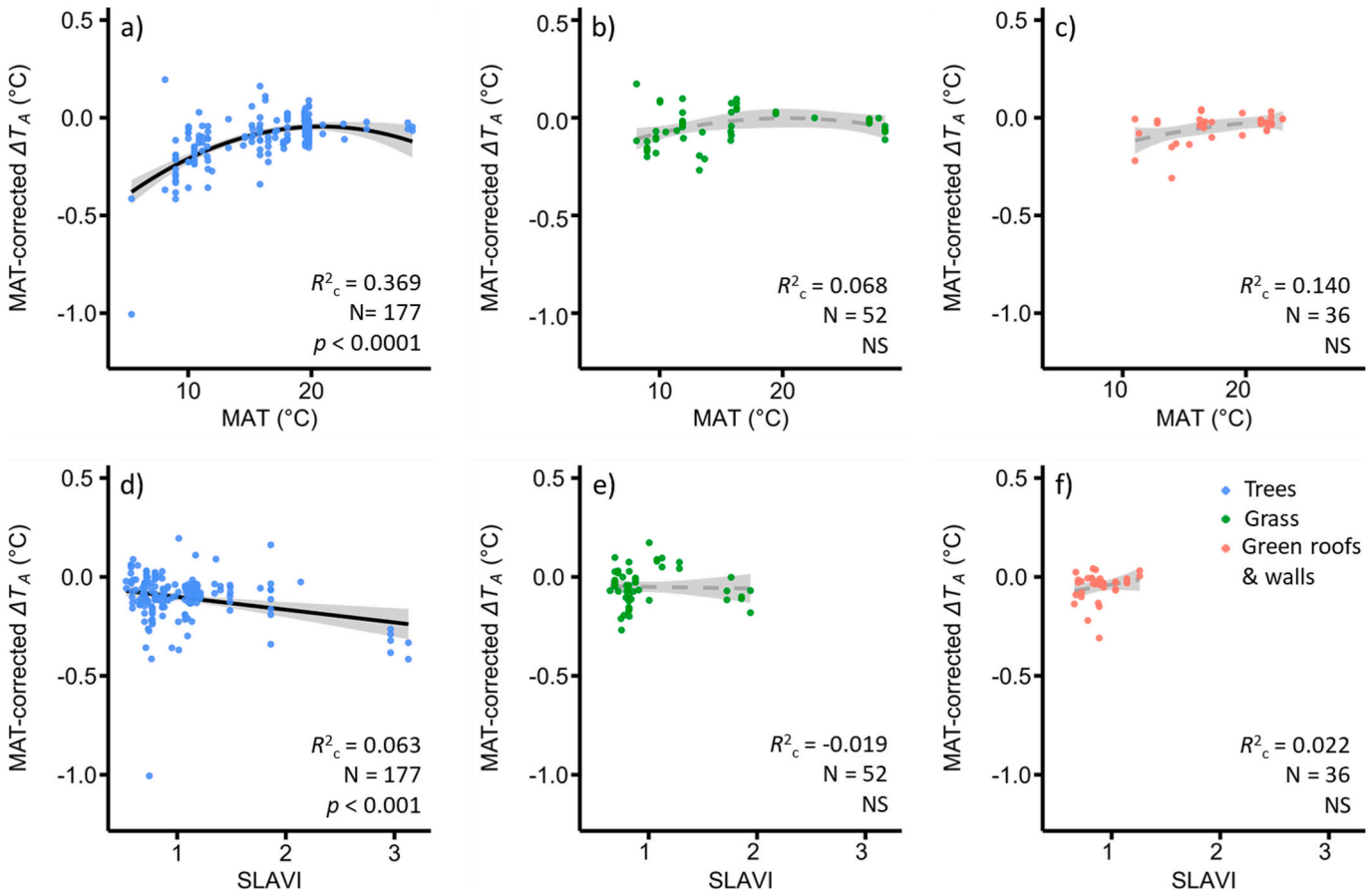

Fig. 6. The fixed effect relationships between MAT-corrected ΔT_A and MAT and SLAVI across UGS types: a & d) trees (light blue; $N = 177$), b & e) grass (green; $N = 52$), e & f) green roofs and walls (light red; $N = 36$). Grey dashed lines present non-significant (NS) interactions between variables.

Water availability through atmospheric humidity, rainfall and irrigation also controls plant growth and consequent evapotranspiration rates that promote UGS cooling effects (Manoli et al., 2019; Nooraei Beidokhti and Moore, 2021; Zhao et al., 2014). In regions with limited water availability (e.g., mean annual precipitation below 1000 mm), UGS cooling effects on LST are more effective in mitigating UHIs due to lower UHI intensity (<0.5 °C) in these areas compared to regions with higher precipitation, where UHI intensity is higher (≥0.5 °C) (Manoli et al., 2019). In our analysis, precipitation did not show a significant interaction with local ΔT_A in the hierarchical model, while other studies have shown a significant relationship between UHIs and precipitation (Gu and Li, 2018; Zhao et al., 2014). Similarly, the response ratio of SMD did not differ significantly with climate zones (Fig. 4e), which is determined by long-term temperature and precipitation patterns. This discrepancy may be due to the limitations of instantaneous in-situ field measurements in capturing the long-term effects of water availability on plant ecophysiology. Contrarily, remotely sensed LSTs provide real-time data with high spatio-temporal resolution and global coverage, allowing for long-term records (Venter et al., 2021; Zhang et al., 2014).

4.3. Effects of plant growth on UGS cooling

Our hierarchical model was designed to account for the major controls of plant functions, before introducing it as a term in the model. Still, SLAVI showed a significant interaction with MAT in explaining the cooling effects of UGS across globally distributed sites (Table 2 & Fig. 5d). SLAVI is a relatively new index for estimating Specific Leaf Area (SLA) from remote sensing imageries (Lymburner et al., 2000), and so limited studies are available for comparison with our SLAVI result (Barati et al., 2011; Morcillo-Pallarés et al., 2019). SLA, which relates to the growth and expansion of plant canopies through the production of new leaf area relative to biomass (Kimball et al., 2002; Liu et al., 2017), can be used to interpret our SLAVI findings here. Across the range of SLAVI values measured here, we consider lower SLAVI values (close to 0.5) and higher SLAVI values (close to 3.1) to indicate smaller photosynthetic capacity and higher plant growth rates, respectively (Fig. 5d) (Lymburner et al., 2000). This result is consistent with previous findings that suggest vegetation growth plays a significant role in the UGS cooling effect (Su et al., 2020). Similarly, previous studies in tundra sites across urban and forest land covers have found a robust positive linear relationship between T_A and SLA together with soil moisture, suggesting that plants with high SLA (e.g., the larger size of trees and leaves with higher photosynthetic capacity) influence global temperature in the long-term (Bjorkman et al., 2018). Sharmin et al. (2023) also demonstrated that SLA determines the cooling benefits of urban trees associated with lowering T_A in surrounding areas. Despite these strong associations between SLA and the cooling effects of plants, such response of T_A to SLA varies depending on the different plant structural characteristics (e.g., functional type, growing size, wood anatomy and leaf colour, shape and thickness) (Liu et al., 2017; Sharmin et al., 2023). Due to the intricate nature of plant characteristics, this study lacks adequate data sources to offer a more precise estimation of the SLAVI response to specific plant traits. Further investigation is, thus, needed to understand how the relationship between T_A and SLAVI is influenced by plant functional traits across plant species that dominate UGS globally (e.g., leaf shape and thickness). Moreover, future research should consider the varying spatial resolutions between remote sensing data (e.g., 30 m pixels) and fine-scale in-situ measurements, as compared here, and how these patterns are underpinned by varying biophysical and biochemical mechanisms.

4.4. Effects of urban characteristics on UGS cooling

Urban characteristics including NDBI and human population did not show a significant relationship with observed T_A measurements in the hierarchical model (Table 2). Although large and dense cities tend to emit more anthropogenic heat that causes increased urban temperature with population, urban characteristics alone are not sufficient to regulate urban temperatures (Manoli et al., 2019). While background climate plays a crucial role in controlling UGS cooling effects by influencing plant functions, particularly evapotranspiration, urban characteristics contribute to temperature regulation by affecting surface convection efficiency associated with urban fabric and density (Manoli et al., 2019). Meanwhile, many local scale studies have reported a strong positive relationship between urban surface temperature and NDBI obtained from various sources of remote sensing data including Landsat 5–8 and MODIS (Purio et al., 2022; Zhang et al., 2009). Although we expected this observation in our study, differences in resolution between in-situ measurements and remotely sensed data may interfere with this relationship. The effect of urban characteristics was also likely captured by vegetation indices, whereby the addition of urban characteristics did not explain additional variation in the temperature observations. Future research could use finer-resolution remote sensing observations to account for direct links between urban temperature and site-specific conditions such as the structure and composition of built-up areas, and more strategically pair neighbouring grey, urban, impervious surfaces and UGS temperatures.

4.5. Effects of different UGS types on urban cooling

The cooling effects associated with background climate and plant characteristics identified here differ significantly among UGS types (trees, grass and green roofs and walls) (Fig. 6). Trees dominated the overall cooling effects of UGS and were better explained by MAT and SLAVI relationships compared to other UGS types such as grass and green roofs and walls. Consistent with our findings, other studies have demonstrated that trees with dense canopies are more efficient in urban cooling compared to grass and shrubs, attributed to greater shading and evapotranspiration cooling (Richards et al., 2020; Su et al., 2022). Brown et al. (2015) reported that using trees for shade is highly effective in regulating T_A, even surpassing plant transpiration. In contrast, grassland exhibited reduced cooling effects and even caused warming effects during the daytime (i.e., $\Delta T_A > 0$) (Su et al., 2020, 2022; Yu et al., 2018). Overall, our analysis highlights trees are considered the most beneficial UGS type for cooling local T_A through shading and evapotranspiration (Zupancic and Bulthuis, 2015) in comparison with other UGS types, grass and green roofs and walls. Our analysis, however, found no clear relationships between ΔT_A with MAT and SLAVI for grass and green roofs and walls due to the relatively smaller measured areas in green roofs and walls and limited plant growth in grasslands, which potentially hinders the evaluation of these relationships.

4.6. Limitations and future research

Our analysis of in-situ ΔT_A from globally distributed sites is based on a compiled dataset from selected peer-reviewed journal papers but is limited by scope and data availability. In the systematic literature review, only peer-reviewed journal papers written in English were included, potentially resulting in the data loss of literature in other languages. The primary bias of this study is that the majority of ΔT_A (total $N = 265$) is situated in temperate climate regions (73.6 %), while cold (continental), dry and tropical climates are underrepresented at 12.5 %, 8.7 % and 5.3 %, respectively. The majority of ΔT_A measurements were from Asia (50.2 %), followed by Europe (21.9 %), South America (21.9 %), North America (4.5 %) and Oceania (1.5 %) (Fig. S2). Additionally, there is a lack of published studies measuring in-situ ΔT_A of UGS in Africa and cold boreal regions (e.g., northern Canada, northern Scandinavia and Russia). Further research on the global-scale cooling effects of UGS should expand to include broader cities, cold boreal and tundra regions and the global south (including African countries). While there is a lack of consideration for the influence of UGS spatial composition and configuration on temperature, our study aimed to synthesise local cooling effects on a global scale to test general relationships, rather than focusing on context-specific conditions such as UGS structure and species within cities. Future studies in remote sensing explore the impact of spatial composition and patterns of UGS on temperature on a global scale. To enhance our understanding of these effects on a global scale, future research should employ standardised methodologies to systematically measure temperatures and explore the interactive effects of different climate zones, plant traits, and urbanisation gradients. For instance, standardised methodologies could be designated at specific locations such as urban centres, residential areas and parks. The same measurement instruments and heights (e.g., 1.5 m above the ground) should be used, as well as consistent data recording intervals (e.g., every minute or hourly) and periods (daily, monthly or yearly).

5. Conclusion

This study aimed to identify the cooling effects of UGS according to background climate, plant and urban characteristics across different UGS types and globally distributed sites. We found trees to be 2–3 times more effective in reducing local T_A compared to grass and green roofs and walls. Cooling benefits are most pronounced at lower MATs and with higher SLAVIs, while urban characteristics such as the human population and NDBI did not show statistical significance. Importantly, trees predominantly drive the overall cooling effects in UGS, exhibiting the most significant cooling impact across UGS types, especially in regions with milder climates and robust tree growth. These findings reinforce the significance of background temperature and plant growth on UGS cooling benefits, highlighting the crucial role of trees in globally mitigating urban heat. Understanding how UGS effectiveness varies based on background climates and plant traits across cities worldwide is essential to regulate the severity of UHI effects, particularly amid rising extreme weather. Further investigation into the global impact of urban trees and their constraints, on UHI intensity under changing extreme weather scenarios is needed to fully appreciate their role in mitigating the urban heat.

CRediT authorship contribution statement

Alice S. A. Johnston: Conceptualisation, Methodology; Jiyoung Kim, Alice S. A. Johnston and Abdou Khouakhi: Data curation, Jiyoung Kim and Alice S. A. Johnston: Formal analysis; Jiyoung Kim and Alice S. A. Johnston: Writing original draft preparation; Jiyoung Kim: Visualisation, investigation; Alice S. A. Johnston, Abdou Khouakhi and Ronald Corstanje: Supervision; Alice S. A. Johnston: Validation; Alice S. A. Johnston and Abdou Khouakhi: Reviewing and editing; Ronald Corstanje: Reviewing.

Code availability

The R code used for analysis during the current study is available at https://zenodo.org/records/10153861. The Python code used to extract vegetation indices is publicly available at https://zenodo.org/records/10153861, with sources provided in the methods section of this article.

Declaration of competing interest

The authors declare that they have no known competing financial interests or personal relationships that could have appeared to influence the work reported in this paper.

Data availability

Sunrise and sunset times are obtained from https://www.sunrise-and-sunset.com/en/sun (accessed on 4 October 2021). Background climate data are collected from the World Bank Group (https://climateknowledgeportal.worldbank.org/; accessed on 21 September 2021) and the Climate Data (https://en.climate-data.org/; accessed on 28 October 2023). Landsat remote sensing data for Plant and urban characteristics are available Earth Engine Data Catalog (https://developers.google.com/earth-engine/datasets/catalog/landsat; accessed on 7 February 2022). The human population data are available at https://citypopulation.de/ (accessed on 30 April 2023). The dataset used for analysis in the R and Python codes during the current study is available at https://zenodo.org/records/10154151.

Acknowledgements

AJ and RC were supported by a Natural Environment Research Council grant (NE/W002906/1). We thank Joanna Zawadzka for helpful discussions and three anonymous reviewers, whose feedback greatly improved the manuscript.

Appendix A. Supplementary data

Supplementary data to this article can be found online at https://doi.org/10.1016/j.scitotenv.2023.168494.

References

Adab, H., Kanniah, K.D., Beringer, J., 2016. Estimating and up-scaling fuel moisture and leaf dry matter content of a temperate humid forest using multi resolution remote sensing data. Remote Sens. (Basel) 8, 961. https://doi.org/10.3390/rs8110961.

Balany, F., Ng, A.W.M., Muttil, N., Muthukumaran, S., Wong, M.S., 2020. Green infrastructure as an urban heat island mitigation strategy—a review. Water 12, 3577. https://doi.org/10.3390/w12123577.

Barati, S., Rayegani, B., Saati, M., Sharifi, A., Nasri, M., 2011. Comparison the accuracies of different spectral indices for estimation of vegetation cover fraction in sparse vegetated areas. Egypt. J. Remote Sens. Space Sci. 14, 49–56. https://doi.org/10.1016/j.ejrs.2011.06.001.

Bartesaghi Koc, C., Osmond, P., Peters, A., 2018. Evaluating the cooling effects of green infrastructure: a systematic review of methods, indicators and data sources. Sol. Energy 166, 486–508. https://doi.org/10.1016/j.solener.2018.03.008.

Bartesaghi-Koc, C., Osmond, P., Peters, A., 2020. Quantifying the seasonal cooling capacity of 'green infrastructure types' (GITs): an approach to assess and mitigate surface urban heat island in Sydney, Australia. Landsc. Urban Plan. 203, 103893 https://doi.org/10.1016/j.landurbplan.2020.103893.

Bartoń, K., 2023. Package "MuMIn" title multi-model inference, R package version 1.47.5. https://CRAN.R-project.org/package=MuMIn (accessed on 5 February 2023).

Bates, D., Mächler, M., Bolker, B.M., Walker, S.C., 2015. Fitting linear mixed-effects models using lme4. J. Stat. Softw. 67, 1–48. https://doi.org/10.18637/jss.v067.i01.

Beck, H.E., Zimmermann, N.E., McVicar, T.R., Vergopolan, N., Berg, A., Wood, E.F., 2018. Present and future Köppen-Geiger climate classification maps at 1-km resolution. Sci. Data 5, 180214. https://doi.org/10.1038/sdata.2018.214.

Biudes, M.S., Machado, N.G., Danelichen, V.H.M., Souza, M.C., Vourlitis, G.L., Nogueira, J.S., 2014. Ground and remote sensing-based measurements of leaf area index in a transitional forest and seasonal flooded forest in Brazil. Int. J. Biometeorol. 58, 1181–1193. https://doi.org/10.1007/s00484-013-0713-4.

Bjorkman, A.D., Myers-Smith, I.H., Elmendorf, S.C., Normand, S., Rüger, N., Beck, P.S.A., Blach-Overgaard, A., Blok, D., Cornelissen, J.H.C., Forbes, B.C., Georges, D., Goetz, S.J., Guay, K.C., Henry, G.H.R., HilleRisLambers, J., Hollister, R.D., Karger, D. N., Kattge, J., Manning, P., Weiher, E., 2018. Plant functional trait change across a warming tundra biome. Nature 562, 57–62. https://doi.org/10.1038/s41586-018-0563-7.

Bowler, D.E., Buyung-Ali, L., Knight, T.M., Pullin, A.S., 2010. Urban greening to cool towns and cities: a systematic review of the empirical evidence. Landsc. Urban Plan. 97, 147–155. https://doi.org/10.1016/j.landurbplan.2010.05.006.

Brown, R.D., Vanos, J., Kenny, N., Lenzholzer, S., 2015. Designing urban parks that ameliorate the effects of climate change. Landsc. Urban Plan. 138, 118–131. https://doi.org/10.1016/j.landurbplan.2015.02.006.

Coronel, S.A., Feldman, S.R., Jozami, E., Facundo, K., Piacentini, R.D., Dubbeling, M., Escobedo, F.J., 2015. Effects of urban green areas on air temperature in a medium-sized Argentinian city. AIMS Environ. Sci. 2, 803–826. https://doi.org/10.3934/environsci.2015.3.803.

Estoque, R.C., Murayama, Y., Myint, S.W., 2017. Effects of landscape composition and pattern on land surface temperature: an urban heat island study in the megacities of Southeast Asia. Sci. Total Environ. 577, 349–359. https://doi.org/10.1016/j.scitotenv.2016.10.195.

Gartland, L., 2008. Heat Islands: Understanding and Mitigating Heat in Urban Areas in the UK and USA. Earthscan.

Gu, Y., Li, D., 2018. A modeling study of the sensitivity of urban heat islands to precipitation at climate scales. Urban Clim. 24, 982–993. https://doi.org/10.1016/j.uclim.2017.12.001.

Huete, A.R., 1988. A soil-adjusted vegetation index (SAVI). Remote Sens. Environ. 25, 295–309. https://doi.org/10.1016/0034-4257(88)90106-X.

Iio, A., Hikosaka, K., Anten, N.P.R., Nakagawa, Y., Ito, A., 2014. Global dependence of field-observed leaf area index in woody species on climate: a systematic review. Glob. Ecol. Biogeogr. 23, 274–285. https://doi.org/10.1111/geb.12133.

Imhoff, M.L., Zhang, P., Wolfe, R.E., Bounoua, L., 2010. Remote sensing of the urban heat island effect across biomes in the continental USA. Remote Sens. Environ. 114, 504–513. https://doi.org/10.1016/j.rse.2009.10.008.

Kimball, B.A., Kobayashi, K., Bindi, M., 2002. Responses of agricultural crops to free-air CO_2 enrichment. Adv. Agron. 77, 293–368. https://doi.org/10.1016/S0065-2113(02)77017-X.

Krayenhoff, E.S., Moustaoui, M., Broadbent, A.M., Gupta, V., Georgescu, M., 2018. Diurnal interaction between urban expansion, climate change and adaptation in US cities. Nat. Clim. Change 8, 1097–1103. https://doi.org/10.1038/s41558-018-0320-9.

Li, P., Xiao, C., Feng, Z., 2018. Mapping rice planted area using a new normalized EVI and SAVI (NVI) derived from landsat-8 OLI. IEEE Geosci. Remote Sens. Lett. 15, 1822–1826. https://doi.org/10.1109/LGRS.2018.2865516.

Li, D., Liao, W., Rigden, A.J., Liu, X., Wang, D., Malyshev, S., Shevliakova, E., 2019. Urban heat island: aerodynamics or imperviousness? Sci. Adv. 5, eaau4229. https://doi.org/10.1126/sciadv.aau4299.

Liu, M., Wang, Z., Li, S., Lü, X., Wang, X., Han, X., 2017. Changes in specific leaf area of dominant plants in temperate grasslands along a 2500-km transect in northern China. Sci. Rep. 7, 10780. https://doi.org/10.1038/s41598-017-11133-z.

Lymburner, L., Beggs, P.J., Jacobson, C.R., 2000. Estimation of canopy-average surface-specific leaf area using LandsatTM data. Photogramm. Eng. Remote Sens. 66, 183–191.

Manoli, G., Fatichi, S., Schläpfer, M., Yu, K., Crowther, T.W., Meili, N., Burlando, P., Katul, G.G., Bou-Zeid, E., 2019. Magnitude of urban heat islands largely explained by climate and population. Nature 573, 55–60. https://doi.org/10.1038/s41586-019-1512-9.

Marando, F., Heris, M.P., Zulian, G., Udías, A., Mentaschi, L., Chrysoulakis, N., Parastatidis, D., Maes, J., 2022. Urban heat island mitigation by green infrastructure in European functional urban areas. Sustain. Cities Soc. 77, 103564 https://doi.org/10.1016/j.scs.2021.103564.

Montero, D., 2021. Eemont: a Python package that extends Google Earth Engine. J. Open Source Softw. 6, 3168. https://doi.org/10.21105/joss.03168.

Mora, C., Dousset, B., Caldwell, I.R., Powell, F.E., Geronimo, R.C., Bielecki, C.R., Counsell, C.W.W., Dietrich, B.S., Johnston, E.T., Louis, L.V., Lucas, M.P., Mckenzie, M.M., Shea, A.G., Tseng, H., Giambelluca, T.W., Leon, L.R., Hawkins, E., Trauernicht, C., 2017. Global risk of deadly heat. Nat. Clim. Chang. 7, 501–506. https://doi.org/10.1038/nclimate3322.

Morcillo-Pallarés, P., Rivera-Caicedo, J.P., Belda, S., De Grave, C., Burriel, H., Moreno, J., Verrelst, J., 2019. Quantifying the robustness of vegetation indices through global sensitivity analysis of homogeneous and forest leaf-canopy radiative transfer models. Remote Sens. (Basel) 11, 2418. https://doi.org/10.3390/rs11202418.

Nooraei Beidokhti, A., Moore, T.L., 2021. The effects of precipitation, tree phenology, leaf area index, and bark characteristics on throughfall rates by urban trees: a meta-data analysis. Urban For. Urban Green. 60, 127052 https://doi.org/10.1016/j.ufug.2021.127052.

Page, M.J., McKenzie, J.E., Bossuyt, P.M., Boutron, I., Hoffmann, T.C., Mulrow, C.D., Shamseer, L., Tetzlaff, J.M., Akl, E.A., Brennan, S.E., Chou, R., Glanville, J., Grimshaw, J.M., Hróbjartsson, A., Lalu, M.M., Li, T., Loder, E.W., Mayo-Wilson, E., McDonald, S., Moher, D., 2021. The PRISMA 2020 statement: an updated guideline for reporting systematic reviews. Syst. Rev. 10, 89. https://doi.org/10.1186/s13643-021-01626-4.

Parishwad, G.V., Bhardwaj, R.K., Nema, V.K., 1998. Prediction of monthly-mean hourly relative humidity, ambient temperature, and wind velocity for India. Renew. Energy 13, 363–380. https://doi.org/10.1016/S0960-1481(98)00010-X.

Purio, M.A., Yoshitake, T., Cho, M., 2022. Assessment of intra-urban heat island in a densely populated city using remote sensing: a case study for Manila City. Remote Sens. (Basel) 14, 5573. https://doi.org/10.3390/rs14215573.

R Core Team, 2022. R: A Language and Environment for Statistical Computing. R Foundation for Statistical Computing, Vienna, Austria. https://www.R-project.org/ (accessed on 10 October 2021).

Richards, D.R., Fung, T.K., Belcher, R.N., Edwards, P.J., 2020. Differential air temperature cooling performance of urban vegetation types in the tropics. Urban For. Urban Green. 50, 126651 https://doi.org/10.1016/j.ufug.2020.126651.

Rohatgi, Ankit, 2022. WebPlotDigitizer (version 4.6). https://automeris.io/WebPlotDigitizer. September, 2022, Pacifica, CA, USA. (accessed on 6 October 2021).

Saaroni, H., Amorim, J.H., Hiemstra, J.A., Pearlmutter, D., 2018. Urban Green Infrastructure as a tool for urban heat mitigation: survey of research methodologies and findings across different climatic regions. Urban Clim. 24, 94–110. https://doi.org/10.1016/j.uclim.2018.02.001.

Sharmin, M., Tjoelker, M.G., Pfautsch, S., Esperón-Rodriguez, M., Rymer, P.D., Power, S. A., 2023. Tree traits and microclimatic conditions determine cooling benefits of urban trees. Atmosphere 14, 606. https://doi.org/10.3390/atmos14030606.

Shi, Z., Li, X., Hu, T., Yuan, B., Yin, P., Jiang, D., 2023. Modeling the intensity of surface urban heat island based on the impervious surface area. Urban Clim. 49, 101529 https://doi.org/10.1016/j.uclim.2023.101529.

Su, Y., Liu, L., Liao, J., Wu, J., Ciais, P., Liao, J., He, X., Liu, X., Chen, X., Yuan, W., Zhou, G., Lafortezza, R., 2020. Phenology acts as a primary control of urban vegetation cooling and warming: a synthetic analysis of global site observations. Agric. For. Meteorol. 280, 107765 https://doi.org/10.1016/j.agrformet.2019.107765.

Su, Y., Wu, J., Zhang, C., Wu, X., Li, Q., Liu, L., Bi, C., Zhang, H., Lafortezza, R., Chen, X., 2022. Estimating the cooling effect magnitude of urban vegetation in different climate zones using multi-source remote sensing. Urban Clim. 43, 101155 https://doi.org/10.1016/j.uclim.2022.101155.

Unger, J., Gál, T., Rakonczai, J., Mucsi, L., Szatmári, J., Tobak, Z., Van Leeuwen, B., Fiala, K., 2009. Air temperature versus surface temperature in urban environment. In: The Seventh International Conference on Urban Climate, July, pp. 3–6.

United Nations. Department of Economic and Social Affairs, Population Division, 2019. World Urbanization Prospects the 2018 Revision (ST/ESA/SER.A/420). United Nations, New York.

Varquez, A.C.G., Kanda, M., 2018. Global urban climatology: a meta-analysis of air temperature trends (1960–2009). Npj Clim. Atmos. Sci. 1, 32. https://doi.org/10.1038/s41612-018-0042-8.

Venter, Z.S., Chakraborty, T., Lee, X., 2021. Crowdsourced air temperatures contrast satellite measures of the urban heat island and its mechanisms. Sci. Adv. 7, eabb9569. https://doi.org/10.1126/sciadv.abb9569.

Wang, C., Wang, Z.H., Wang, C., Myint, S.W., 2019. Environmental cooling provided by urban trees under extreme heat and cold waves in U.S. cities. Remote Sens. Environ. 227, 28–43. https://doi.org/10.1016/j.rse.2019.03.024.

Wang, J., Zhou, W., Jiao, M., Zheng, Z., Ren, T., Zhang, Q., 2020. Significant effects of ecological context on urban trees' cooling efficiency. ISPRS J. Photogramm. Remote Sens. 159, 78–89. https://doi.org/10.1016/j.isprsjprs.2019.11.001.

Wilson, E.H., Sader, S.A., 2002. Detection of forest harvest type using multiple dates of LandsatTM imagery. Remote Sens. Environ. 80, 385–396. https://doi.org/10.1016/S0034-4257(01)00318-2.

Winbourne, J.B., Jones, T.S., Garvey, S.M., Harrison, J.L., Wang, L., Li, D., Templer, P.H., Hutyra, L.R., 2020. Tree transpiration and urban temperatures: current understanding, implications, and future research directions. BioScience 70, 576–588. https://doi.org/10.1093/biosci/biaa055.

Yu, Z., Xu, S., Zhang, Y., Jørgensen, G., Vejre, H., 2018. Strong contributions of local background climate to the cooling effect of urban green vegetation. Sci. Rep. 8, 6798. https://doi.org/10.1038/s41598-018-25296-w.

Zha, Y., Gao, J., Ni, S., 2003. Use of normalized difference built-up index in automatically mapping urban areas from TM imagery. Int. J. Remote Sens. 24, 583–594. https://doi.org/10.1080/01431160304987.

Zhang, P., Bounoua, L., Imhoff, M.L., Wolfe, R.E., Thome, K., 2014. Comparison of MODIS land surface temperature and air temperature over the continental USA meteorological stations. Can. J. Remote. Sens. 40, 110–122. https://doi.org/10.1080/07038992.2014.935934.

Zhang, Y., Odeh, I.O.A., Han, C., 2009. Bi-temporal characterization of land surface temperature in relation to impervious surface area, NDVI and NDBI, using a sub-pixel image analysis. Int. J. Appl. Earth Obs. Geoinf. 11, 256–264. https://doi.org/10.1016/j.jag.2009.03.001.

Zhao, L., Lee, X., Smith, R.B., Oleson, K., 2014. Strong contributions of local background climate to urban heat islands. Nature 511, 216–219. https://doi.org/10.1038/nature13462.

Zhao, L., Oppenheimer, M., Zhu, Q., Baldwin, J.W., Ebi, K.L., Bou-Zeid, E., Guan, K., Liu, X., 2018. Interactions between urban heat islands and heat waves. Environ. Res. Lett. 13, 034003 https://doi.org/10.1088/1748-9326/aa9f73.

Zhou, D., Xiao, J., Bonafoni, S., Berger, C., Deilami, K., Zhou, Y., Frolking, S., Yao, R., Qiao, Z., Sobrino, J.A., 2019. Satellite remote sensing of surface urban heat islands: progress, challenges, and perspectives. Remote Sens. (Basel) 11, 48. https://doi.org/10.3390/rs11010048.

Zupancic, T., Bulthuis, M., 2015. The Impact of Green Space on Heat and Air Pollution in Urban Communities: The Meta-narrative Systematic Review. Canadian Electronic Library, Ottawa, Ontario.

Greater local cooling effects of trees across globally distributed urban green spaces

Kim, Jiyoung

2024-02-10

Kim J, Khouakhi A, Corstanje R, Johnston AS. (2024) Greater local cooling effects of trees across globally distributed urban green spaces. Science of The Total Environment, Volume 911, February 2024, Article number 168494

https://doi.org/10.1016/j.scitotenv.2023.168494